Some Aspects on Hybrid Wideband Transceiver Design for mmWave Communication Systems

Marcin Iwanow*†, Nikola Vucic*, Mario H. Castañeda*, Jian Luo*, Wen Xu * and Wolfgang Utschick†
*Huawei Technologies Duesseldorf GmbH, Munich, Germany
Email: {iwanow.marcin, nikola.vucic, mario.castaneda, jianluo}@huawei.com
†Associate Institute for Signal Processing, Technische Universität München, Germany
Email: utschick@tum.de

***Abstract*—In this paper, the problem of designing a multicarrier transceiver for single-link mmWave transmission is considered. Assuming the hybrid beamforming approach with multiple data streams, it is shown how the common wideband analog beamformer can be optimized together with digital multiple-input, multiple-output precoders and receive equalizers which operate on per-subcarrier basis. For this purpose, two approaches originally constructed for narrowband systems are extended to wideband, and several simplifications for solving the optimization problems are made. Their evaluation is performed on an proposed statistical mmWave channel model and by utilizing measured channels.**

I. Introduction

In recent years, the utilization of new frequency bands in the mmWave region for the 5th generation (5G) of cellular networks has drawn significant attention in the industry and academia [1], [2]. Exploitation of large channel bandwidths at high frequencies is seen as one of the key enablers in addressing the extremely challenging 5G requirements, particularly in terms of anticipated data rates [3]. However, moving to higher portions of the radio spectrum requires considerable changes in both lower and higher layers of the protocol stack.

Currently, the first commercial products in the license-free V-band appear in the market following the IEEE 802.11ad standard [4]. The new IEEE802.11ay standard is expected to provide significant improvements in achievable data rates and supported use cases. In parallel, several research initiatives have started with the goal of exploiting other mmWave frequency bands (K_a band, E-band, etc.) and designing an integrated 5G cellular wireless system (c.f. [5]).

In this work, we analyze the problem of jointly designing the transmitter and the receiver in a multi-stream, multicarrier mmWave system. The underlying architecture follows the hybrid beamforming principle, where analog processing (beamforming) is performed in order to reduce the number of required analog-to-digital and digital-to-analog chains (ADCs/DACs) [6]. The considered system model is recognized in the community as one of the candidate solutions for 5G mmWave radio access networks (RAN) and backhaul.

A. State of the Art on mmWave Precoding/Equalization

As a consequence of the high frequencies, large bandwidths and the high number of antennas at both the transmitter and receiver expected in mmWave systems, performing fully digital beamforming might not be practical. Although digital beamforming offers the maximum degree of flexibility for the transceiver design, it results in high complexity, cost and energy consumption when operating at mmWave frequencies due to the need of a large amount of radio frequency (RF) chains including high resolution converters (ADCs/DACs) with a high sampling rate.

To address this aspect, one can consider decreasing the resolution of the converters, for instance of the ADCs at the receiver side [7]. Another possibility consists of reducing the number of RF chains (leading to less converters) by employing hybrid beamforming [8]–[11]. By performing part of the beamforming operations in the analog domain, hybrid beamforming is able to provide a trade-off between performance and complexity/energy consumption. The hybrid beamforming architecture has also been considered for massive MIMO systems [12]–[14] due to the use of a massive amount of antennas at the base station.

All the works assume, however, a narrowband model, i.e., a frequency flat channel. As pointed out in [15], the transceiver design for broadband systems is still an open research problem. The design of hybrid beamforming for multicarrier systems has not been studied extensively yet – it has been only considered in a few works [16]–[19]. A simple extension of the hybrid beamforming algorithms for the narrowband system is not possible for a practical reason – the analog beamformer cannot vary among the subcarriers, i.e., it is fixed for all the entire bandwidth [17]–[19]. In the following we briefly review the prior work for broadband systems.

In [16], the analog beamforming at the transmitter and at the receiver are chosen with the aim of maximizing the average (over all subcarriers) of the largest singular value of the effective channel matrix on each subcarrier. The effective channel matrix on each subcarrier consists of the product of the analog receive beamforming matrix, the multiple-input multiple-output (MIMO) channel on each subcarrier and the analog transmit beamforming matrix. For the proposed single stream transmission, the digital beamforming for each subcarrier at the transmitter and receiver are chosen such that they correspond to the right and left singular vectors of the effective channel matrix on each subcarrier, respectively.

The design of hybrid beamforming is studied for a MIMO-OFDM system for single stream transmission in [17], where

the analog and digital beamformers are chosen from quantized codebooks. The optimum choice for the transmit analog and digital beamformers and the receive analog beamformers involves an exhaustive joint search over all possible combinations. To simplify the exhaustive search, a sequential searching algorithm is also proposed in [17], where the best transmit/receive analog beam pairs are first chosen without considering the transmit digital beamforming, which is later selected based on the chosen analog beamformers. In [17], a hybrid beamforming architecture with subarrays is assumed, which is extended to a shared antenna array in [20].

In [18], a multiuser multicarrier system is considered. The authors aim at the hybrid beamforming at the transmitter such that it perfectly matches the performance of a system with fully digital frontend. The authors propose QR-based factorization of the collection of the digital beamforming matrices over all subcarriers and show that a hybrid beamforming architecture with r_{t} RF chains and $2r_{\mathrm{t}}(N_{\mathrm{tx}} - r_{\mathrm{t}} + 1)$ infinite resolution phase shifters can match the performance of an system with fully digital frontend. r_{t} and N_{tx} are the rank of the digital beamforming matrices and the number of transmitter antennas, respectively. Note that for a standard hybrid structure only one phase shifter per antenna is assumed for each RF chain.

The design of the hybrid beamforming with multiple streams for wideband mmWave systems has been studied also in [19] under the assumption of limited feedback. The analog beamformers are taken from a codebook. The case when the digital beamformers are also considered to be taken from a codebook is also investigated. The work in [19] provides insight into the design of the codebooks.

B. Contributions

Differently from the previous works which consider single stream transmission or assume codebook based approaches, we aim at optimal linear multicarrier MIMO transceiver design based on hybrid beamforming.

The problem of interest is involved due to specific constraints on the analog filters, which are composed of phase shifters and should be fixed for the entire bandwidth. The setting we study is in compliance with the often assumed time-division-duplex (TDD) assumption for a small mmWave cell. We show how two algorithms originally constructed for the narrowband case, namely the compressed sensing based (CS) and the block coordinate descent (BCD) strategies [21], [30], respectively, can be extended to support the multicarrier case. Having in mind specific mmWave sparse channel characteristics, we analyse several low-complexity alternatives to the (sub)-optimized designs, and examine the gap with respect to the fully digital transceiver design. A statistical spatio-temporal channel model is used in our analysis to evaluate the proposed solutions. Finally, the performance of the algorithms is tested with data obtained in a measurement campaign.

C. Outline of the Paper

The rest of the paper is organized as follows. After the notation convention, Section II gives a detailed description of the system model. The assumed mmWave channel model is elaborated in Section III. In Section IV, the mathematical descriptions of the considered problems are presented, followed by the proposed solutions. Finally, Section V shows simulation results of the examined strategies for the assumed statistical channel model, as well as for a set of channel measurements.

D. Notation

We use lower case boldface characters to denote (column) vectors and capital boldface characters to denote matrices. We denote identity matrix of size $N \times N$ with $\boldsymbol{I}_N$. $(\cdot)^{\mathrm{T}}$, $(\cdot)^{\mathrm{H}}$, and $(\cdot)^{\dagger}$ denote transpose, conjugate transpose, and Moore-Penrose pseudoinverse, respectively. We denote the linear convolution with $*$. We use $\mathrm{tr}(\boldsymbol{A})$, $\|\boldsymbol{A}\|_{\mathrm{F}}$, $\|\boldsymbol{A}\|_2$ for the trace, the Frobenius norm, and the 2-norm of the matrix $\boldsymbol{A}$, respectively. The (m,n)-th entry of the matrix $\boldsymbol{A}$ is denoted with $[\boldsymbol{A}]_{(m,n)}$. The expected value of a random variable is denoted with $\mathrm{E}[\cdot]$, $\boldsymbol{b} \sim \mathcal{N}_{\mathbb{C}}(\boldsymbol{a}, \boldsymbol{A})$ means that the random variable $\boldsymbol{b}$ follows a circular complex Gaussian distribution with mean $\boldsymbol{a}$ and covariance matrix $\boldsymbol{A}$. $b \sim U[a_1, a_2]$ means, that random variable b follows the uniform distribution within $[a_1, a_2]$. If Ω is a set, we denote the cardinality of Ω with $|\Omega|$; otherwise, this operator stands for the absolute value.

II. System Model

We consider a point-to-point OFDM setup consisting of one transmitter (Tx) with N_{tx} antennas and one receiver (Rx) with N_{rx} antennas. The frontend of both Tx and Rx has hybrid a structure as shown in Fig. 1. The number of RF chains in the transmitter and in the receiver is $N_{\mathrm{tx}}^{\mathrm{RF}}$ and $N_{\mathrm{rx}}^{\mathrm{RF}}$, respectively and $N_{\mathrm{tx}}^{\mathrm{RF}} \leq N_{\mathrm{tx}}$, $N_{\mathrm{rx}}^{\mathrm{RF}} \leq N_{\mathrm{rx}}$.

The system is operating within a bandwidth substantially exceeding the coherence bandwidth of the channel, i.e., the channel is wideband/frequency selective. In the time domain, this means that the channel impulse response (CIR) consists of multiple taps [22, Chapter 2]. If the channel is sampled with a sampling rate $f_s = \frac{1}{T_s}$, it can be seen as an FIR filter. If the order of the filter (determined by the maximum delay spread) is D and the channel is assumed to be linear time-invariant (LTI), the symbol received at the time instance nT_s reads as

$$\boldsymbol{y}[n] = \sum_{d=0}^{D} \boldsymbol{H}[d]\boldsymbol{x}[n-d] + \boldsymbol{\eta}[n], \tag{1}$$

where $\boldsymbol{y}[n] \in \mathbb{C}^{N_{\mathrm{rx}}}$ is the vector received at the time instance nT_s, $\boldsymbol{x}[n-d] \in \mathbb{C}^{N_{\mathrm{tx}}}$ the vector transmitted at the time instance $(n-d)T_s$, $\boldsymbol{H}[d] \in \mathbb{C}^{N_{\mathrm{tx}} \times N_{\mathrm{tx}}}$ the CIR sampled at dT_s, and $\boldsymbol{\eta}[n] \in \mathbb{C}^{N_{\mathrm{rx}}}$ is the white noise with $\boldsymbol{\eta}[n] \sim \mathcal{N}_{\mathbb{C}}(\boldsymbol{0}, \sigma_{\eta}^2 \boldsymbol{I}_{N_{\mathrm{rx}}})$.

Using multiple subcarriers for transmission allows to parallelize the frequency-selective channel into a set of frequency-flat channels [23]. Then, for each subcarrier k we have

$$\boldsymbol{y}_k = \boldsymbol{H}_k \boldsymbol{x}_k + \boldsymbol{\eta}_k, \quad k \in \{1, \ldots, N_{\mathrm{subc}}\}, \tag{2}$$

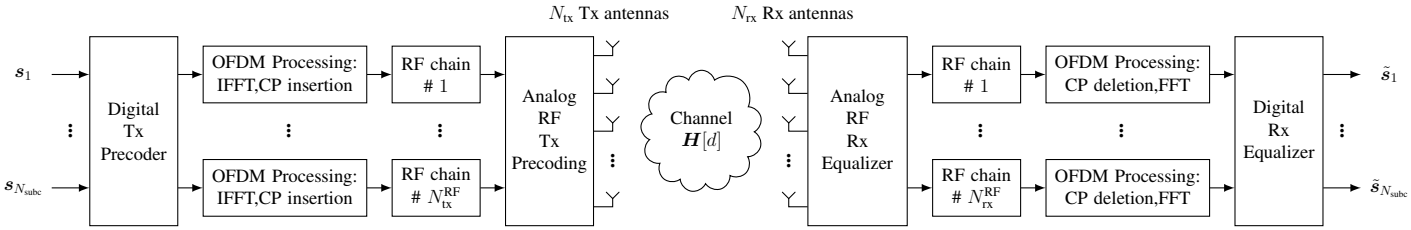

Fig. 1. System model

where $\boldsymbol{y}_k \in \mathbb{C}^{N_{\text{rx}}}$ is the vector received on the k-th subcarrier, $\boldsymbol{x}_k \in \mathbb{C}^{N_{\text{tx}}}$ the vector transmitted on the k-th subcarrier, $\boldsymbol{H}_k \in \mathbb{C}^{N_{\text{tx}} \times N_{\text{tx}}}$ the channel on the k-th subcarrier, and $\boldsymbol{\eta}_k \in \mathbb{C}^{N_{\text{rx}}}$ is the white noise with $\boldsymbol{\eta}_k \sim \mathcal{N}_{\mathbb{C}}(\boldsymbol{0}, \sigma_\eta^2 \boldsymbol{I}_{N_{\text{rx}}})$.

In the paper, we consider linear precoding at the transmitter and linear combining at the receiver. If the transmission carries N_{s} streams, the estimated symbol vector can be written as

$$\tilde{\boldsymbol{s}}_k = \boldsymbol{G}_k^{\text{H}} \boldsymbol{H}_k \boldsymbol{P}_k \boldsymbol{s}_k + \boldsymbol{G}_k^{\text{H}} \boldsymbol{\eta}_k, \quad k \in \{1, \ldots, N_{\text{subc}}\}, \tag{3}$$

where $\boldsymbol{x}_k$ in (2) has been replaced by the symbol vector $\boldsymbol{s}_k \in \mathbb{C}^{N_{\text{s}}}$ precoded with $\boldsymbol{P}_k \in \mathbb{C}^{N_{\text{tx}} \times N_{\text{s}}}$. The matrix $\boldsymbol{G}_k \in \mathbb{C}^{N_{\text{rx}} \times N_{\text{s}}}$ is used for linearly combining the received signals. The per-subcarrier power constraint is ensured by the condition $\|\boldsymbol{P}_k\|_{\text{F}}^2 \leq \frac{P_{\text{tx}}}{N_{\text{subc}}}$, where P_{tx} is the total transmit power.

The hybrid structure of the frontends imposes additional constraints for the precoding and combining matrices. The digital precoding at the transmitter unit is followed by analog precoding and analog combining is followed by digital combining at the receiver (cf. Fig. 1). The analog precoding and combining is usually realized in hardware by means of interconnecting a matrix of $N_{\text{tx}}^{\text{RF}} N_{\text{tx}}$ and $N_{\text{rx}}^{\text{RF}} N_{\text{rx}}$ phase shifters, respectively. Equivalently, the entries of the analog precoding and combining matrices have equal magnitude. Without loss of generality, we set it here to 1. Then, the precoder and combiner for the k-th subcarrier can be written as

$$\boldsymbol{P}_k = \boldsymbol{P}_{k,A} \boldsymbol{P}_{k,D}, \quad \boldsymbol{P}_{k,A} \in \mathcal{P}_{\mathcal{A}}, \tag{4}$$

$$\boldsymbol{G}_k = \boldsymbol{G}_{k,A} \boldsymbol{G}_{k,D}, \quad \boldsymbol{G}_{k,A} \in \mathcal{G}_{\mathcal{A}}, \tag{5}$$

where $\boldsymbol{P}_{k,A} \in \mathbb{C}^{N_{\text{tx}} \times N_{\text{tx}}^{\text{RF}}}$, $\boldsymbol{G}_{k,A} \in \mathbb{C}^{N_{\text{rx}} \times N_{\text{rx}}^{\text{RF}}}$ are the analog precoding and combining matrices, $\boldsymbol{P}_{k,D} \in \mathbb{C}^{N_{\text{tx}}^{\text{RF}} \times N_{\text{s}}}$ and $\boldsymbol{G}_{k,D} \in \mathbb{C}^{N_{\text{rx}}^{\text{RF}} \times N_{\text{s}}}$ are the digital precoding and combining matrices for the k-th subcarrier. The sets $\mathcal{P}_{\mathcal{A}}$ and $\mathcal{G}_{\mathcal{A}}$ are defined as

$$\mathcal{P}_{\mathcal{A}} = \Big\{ \boldsymbol{\Xi} \in \mathbb{C}^{N_{\text{tx}} \times N_{\text{tx}}^{\text{RF}}} : |[\boldsymbol{\Xi}]_{(i,j)}| = 1 \quad \forall (i,j) \text{ s.t. } i \in \{1, \ldots, N_{\text{tx}}\}, j \in \{1, \ldots, N_{\text{tx}}^{\text{RF}}\} \Big\} \tag{6}$$

$$\mathcal{G}_{\mathcal{A}} = \Big\{ \boldsymbol{\Xi} \in \mathbb{C}^{N_{\text{rx}} \times N_{\text{rx}}^{\text{RF}}} : |[\boldsymbol{\Xi}]_{(i,j)}| = 1 \quad \forall (i,j) \text{ s.t. } i \in \{1, \ldots, N_{\text{rx}}\}, j \in \{1, \ldots, N_{\text{rx}}^{\text{RF}}\} \Big\}. \tag{7}$$

At this point, we assume different analog precoding and combining matrices for each subcarrier in order to derive a baseline solution. We consider the constraint of the analog precoding and combining matrices constant for all subcarriers in Section IV-B.

Specifically for the hybrid transceiver structure, (3) can be rewritten as

$$\tilde{\boldsymbol{s}}_k = \boldsymbol{G}_{k,D}^{\text{H}} \boldsymbol{G}_{k,A}^{\text{H}} \boldsymbol{H}_k \boldsymbol{P}_{k,A} \boldsymbol{P}_{k,D} \boldsymbol{s}_k + \boldsymbol{G}_{k,D}^{\text{H}} \boldsymbol{G}_{k,A}^{\text{H}} \boldsymbol{\eta}_k, \quad k \in \{1, \ldots, N_{\text{subc}}\}, \tag{8}$$

with $\|\boldsymbol{P}_{k,A} \boldsymbol{P}_{k,D}\|_{\text{F}}^2 \leq \frac{P_{\text{tx}}}{N_{\text{subc}}}$. We assume availability of ideal channel state information (CSI) both at the receiver and the transmitter. The objective of the precoding and combining design is the achievable rate of the link with Gaussian signaling (cf. [24])

$$R\left(\boldsymbol{P}_{k,A}, \boldsymbol{P}_{k,D}, \boldsymbol{G}_{k,A}, \boldsymbol{G}_{k,D}\right) = \frac{1}{N_{\text{subc}}} \sum_{k=0}^{N_{\text{subc}}-1} \log_2 \det \left(\boldsymbol{I}_{N_{\text{s}}} + \boldsymbol{R}_{k,\eta}^{-1} \boldsymbol{H}_{k,\text{eff}} \boldsymbol{H}_{k,\text{eff}}^{\text{H}} \right) \tag{9}$$

where the effective channel for k-th subcarrier reads

$$\boldsymbol{H}_{k,\text{eff}} = \boldsymbol{G}_{k,D}^{\text{H}} \boldsymbol{G}_{k,A}^{\text{H}} \boldsymbol{H}_k \boldsymbol{P}_{k,A} \boldsymbol{P}_{k,D}, \tag{10}$$

the noise covariance matrix $\boldsymbol{R}_\eta$ can be expressed as

$$\boldsymbol{R}_{k,\eta} = \sigma_\eta^2 \boldsymbol{G}_{k,D}^{\text{H}} \boldsymbol{G}_{k,A}^{\text{H}} \boldsymbol{G}_{k,A} \boldsymbol{G}_{k,D}, \tag{11}$$

and the normalization by N_{subc} is due to the length of the OFDM symbol.

III. Channel Model

For the moment, there is no common agreement about the parameters for mmWave outdoor channel. The following assumpions are frequently used though (e.g., in [25]–[30]):

- The number of paths is significantly lower than for the sub-6GHz frequency band.
- The paths propagate in space and time clusters. There seem to be different views whether propagation in the time cluster implies propagation in the space cluster. The works [27], [28], [30] take this assumption while in [25] it is argued that this is not necessarily the case.

Because of the high number of channel parameters and no common agreement on their modeling, we choose to define a simple model which is compatible with the above two features. The channel parameters are based on [30] and [25] and are described in details in Section V. We use the extended Saleh-Valenzuela model [19], [31], i.e., the MIMO channel sampled

at time instance dT_s is written as a superposition of individual, clustered paths as

$$\boldsymbol{H}[d] = \beta\sqrt{\frac{N_{\text{rx}}N_{\text{tx}}}{L}}\sum_{l=1}^{N_{\text{cl}}}\sum_{r=1}^{N_{\text{path}}^{l}}\alpha_{r,l}p(dT_s-\tau_l-\tau_r)\boldsymbol{a}_{\text{rx}}(\boldsymbol{\theta}_{r,l})\boldsymbol{a}_{\text{tx}}^{\text{H}}(\boldsymbol{\phi}_{r,l}), \tag{12}$$

where N_{cl} is the number of time clusters, N_{path}^{l} is the number of paths in the l-th cluster, $\alpha_{r,l}$ is the path gain for the r-th path in the l-th cluster (including the antenna gain), τ_l is the delay of the l-th cluster, τ_r is the relative delay w.r.t. the cluster delay of the r-th path within the cluster. $\boldsymbol{\theta}_{r,l} = [\kappa_{r,l}^{\theta}, \zeta_{r,l}^{\theta}]$ is the direction of arrival (DoA) vector of the r-th path within the l-th cluster, composed from elevation angle $\kappa_{r,l}^{\theta}$ and the azimuth angle $\zeta_{r,l}^{\theta}$. $\boldsymbol{\phi}_{r,l} = [\kappa_{r,l}^{\phi}, \zeta_{r,l}^{\phi}]$ is the direction of departure (DoD) vector of the r-th path within the l-th cluster, composed from the elevation angle $\kappa_{r,l}^{\phi}$ and the azimuth angle $\zeta_{r,l}^{\phi}$. L expresses the path loss between the transmitter and the receiver, and β is a normalization factor such that $\text{E}\left[\sum_{d=-\infty}^{+\infty}\|\boldsymbol{H}[d]\|_{\text{F}}^2\right] = N_{\text{rx}}N_{\text{tx}}$. The contribution of the r-th path in the l-th cluster for the channel at the time instance dT_s is evaluated by sampling the transfer function p of the pulse-shaping filter at $dT_s - \tau_l - \tau_r$. The vectors $\boldsymbol{a}_{\text{rx}}$ and $\boldsymbol{a}_{\text{tx}}$ are the antenna array response vectors for the receiver and the transmitter, respectively.

For the rest of our paper, we assume uniform linear arrays (ULA) at both the transmitting and receiving sides. The array response vector for ULA reads as

$$\boldsymbol{a}_{\text{ULA}}([\kappa,\zeta]) = \frac{1}{M}\left[1, e^{j\frac{2\pi}{\lambda}d\sin(\zeta)}, \ldots, e^{j(M-1)\frac{2\pi}{\lambda}d\sin(\zeta)}\right] \tag{13}$$

where M denotes the number of antennas, λ the wavelength of the transmitted/received wave, and d is the spacing of the antenna elements. In our work, we assume half-wavelength antenna elements spacing $d = \frac{\lambda}{2}$. The response is independent of the elevation angle κ and depends only on the azimuth angle ζ.

For the multicarrier setup, the channel matrix $\boldsymbol{H}_k$ at the k-th subcarrier is expressed as

$$\boldsymbol{H}_k = \frac{1}{\sqrt{N_{\text{subc}}}}\sum_{d=0}^{D-1}\boldsymbol{H}[d]\exp\left(\frac{j2\pi k}{N_{\text{subc}}}d\right), \tag{14}$$

where we assume that the number of subcarriers is larger than the number of taps in the CIR, i.e., $N_{\text{subc}} > D$.

IV. Wideband Precoding

In this section, we discuss the design of the hybrid wideband precoding and combining. First we present in Section IV-A a baseline solution which is a straightforward extension of algorithms for the narrowband channel. Although it provides good results, it is not realizable in practice. To this end, in Section IV-B we propose an algorithm which aims on finding a practical hybrid wideband beamforming strategy with affordable complexity.

A. Baseline Solution

As a consequence of setting an individual power constraint for every subcarrier, each k-th component of the sum in the rate expression (9) is a function of an individual set of optimization variables. Consequently, the precoders and combiners are obtained by maximizing the sum rate (9) from the following optimization solution

$$R_{\text{max}} = \frac{1}{N_{\text{subc}}}\sum_{k=0}^{N_{\text{subc}}-1}R_{k,\text{max}} \tag{15}$$

where

$$R_{k,\text{max}} = \max_{\substack{\boldsymbol{P}_{k,A},\boldsymbol{P}_{k,D},\\ \boldsymbol{G}_{k,A},\boldsymbol{G}_{k,D}}} \log_2\det\left(\boldsymbol{I}_{N_{\text{s}}} + \boldsymbol{R}_{k,\eta}^{-1}\boldsymbol{H}_{k,\text{eff}}\boldsymbol{H}_{k,\text{eff}}^{\text{H}}\right)$$
$$\text{s.t.} \quad \|\boldsymbol{P}_{k,A}\boldsymbol{P}_{k,D}\|_{\text{F}}^2 \le \frac{P_{\text{tx}}}{N_{\text{subc}}}$$
$$\boldsymbol{P}_{k,A}\in\mathcal{P}_{\mathcal{A}}, \boldsymbol{G}_{k,A}\in\mathcal{G}_{\mathcal{A}}. \tag{16}$$

We can thus restrict further to solving the rate maximization for the k-th subcarrier individually, namely maximizing $R_{k,\text{max}}$. The problem would have an optimal solution if the precoding and combining were not decomposed into the analog and digital parts. Namely, the precoding and combining should be based on the singular value decomposition (SVD) of the channel matrix $\boldsymbol{H}_k$, followed by waterfilling at the transmitter [32]. In the following we assume uniform power allocation throughout N_S streams.

To solve the problem in (16) we first relax it by discarding the constraints $\boldsymbol{P}_{k,A}\in\mathcal{P}_{\mathcal{A}}$ and $\boldsymbol{G}_{k,A}\in\mathcal{G}_{\mathcal{A}}$. In this way, we can obtain the suboptimal[1] precoding and combining matrices as

$$\boldsymbol{P}_k^{\star} = \boldsymbol{V}_k\left[\boldsymbol{I}_{N_{\text{s}}}\,\boldsymbol{0}_{N_{\text{s}}\times(N_{\text{tx}}-N_{\text{s}})}\right]^{\text{T}},$$
$$\boldsymbol{G}_k^{\star} = \boldsymbol{U}_k\left[\boldsymbol{I}_{N_{\text{s}}}\,\boldsymbol{0}_{N_{\text{s}}\times(N_{\text{rx}}-N_{\text{s}})}\right]^{\text{T}}, \tag{17}$$

where $\boldsymbol{U}_k \in \mathbb{C}^{N_{\text{rx}}\times N_{\text{rx}}}$ and $\boldsymbol{V}_k \in \mathbb{C}^{N_{\text{tx}}\times N_{\text{tx}}}$ are unitary matrices containing the left and right singular vectors of $\boldsymbol{H}_k$, respectively, i.e., $\boldsymbol{H}_k = \boldsymbol{U}_k\boldsymbol{\Sigma}_k\boldsymbol{V}_k^{\text{H}}$. The singular values in $\boldsymbol{\Sigma}_k$ are given in descending order.

It is usually not possible to decompose $\boldsymbol{P}_k^{\star}$ and $\boldsymbol{G}_k^{\star}$ such that $\boldsymbol{P}_k^{\star} = \boldsymbol{P}_{k,A}\boldsymbol{P}_{k,D}$ and $\boldsymbol{G}_k^{\star} = \boldsymbol{G}_{k,A}\boldsymbol{G}_{k,D}$ with the constraints $\boldsymbol{P}_{k,A}\in\mathcal{P}_{\mathcal{A}}$ and $\boldsymbol{G}_{k,A}\in\mathcal{G}_{\mathcal{A}}$. We use the same arguments as in [30] to justify that for the mmWave channel we can decompose the precoders and combiners by solving the following optimization problems:

$$\left(\boldsymbol{P}_{k,A}^{\star},\boldsymbol{P}_{k,D}^{\star}\right) = \underset{\boldsymbol{P}_{k,A},\boldsymbol{P}_{k,D}}{\arg\min} \quad \|\boldsymbol{P}_k^{\star} - \boldsymbol{P}_{k,A}\boldsymbol{P}_{k,D}\|_{\text{F}}$$
$$\text{s.t.} \quad \|\boldsymbol{P}_{k,A}\boldsymbol{P}_{k,D}\|_{\text{F}}^2 \le \frac{P_{\text{tx}}}{N_{\text{subc}}}$$
$$\boldsymbol{P}_{k,A}\in\mathcal{P}_{\mathcal{A}} \tag{18}$$

[1]The solution is not optimal due to the constraint on the number of streams and since no waterfilling is considered.

and

$$\left(\boldsymbol{G}_{k,A}^{\star}, \boldsymbol{G}_{k,D}^{\star}\right) = \underset{\boldsymbol{G}_{k,A}, \boldsymbol{G}_{k,D}}{\arg\min} \quad \|\boldsymbol{G}_{k}^{\star} - \boldsymbol{G}_{k,A}\boldsymbol{G}_{k,D}\|_{\mathrm{F}} \quad \text{s.t.} \quad \boldsymbol{G}_{k,A} \in \mathcal{G}_{\mathcal{A}}. \tag{19}$$

For solving these optimization problems, we use the orthogonal matching pursuit (OMP) algorithm described in [30, Algorithm 1] and the modified block coordinate descent (BCD-SD) algorithm proposed in [21, Section IV].

Note, that after the completion of the BCD-SD algorithm we perform the normalization of the digital precoding matrix

$$\boldsymbol{P}_{k,D}^{\star} = \sqrt{\frac{P_{\mathrm{tx}}}{N_{\mathrm{subc}}}} \frac{\boldsymbol{P}_{k,D}^{\star}}{\|\boldsymbol{P}_{k,A}^{\star}\boldsymbol{P}_{k,D}^{\star}\|_{\mathrm{F}}}. \tag{20}$$

B. Practical solutions

In the previous subsection, we outlined the baseline strategy for designing the hybrid precoding and combining. We observe that solving the optimization problem (16) for each subcarrier k results in different analog precoding and combining matrices for each subcarrier. For the hardware implementation this means a separate set of phase shifters for each frequency bin, which is not practicable in real technical systems. Here we propose a suboptimal solution by adding an additional constraint to (18) and (19), i.e., $\boldsymbol{P}_{k,A}^{\star}$ and $\boldsymbol{G}_{k,A}^{\star}$ remain constant for each subcarrier k.

In order to solve this problem, we propose to jointly design an analog precoder matrix $\boldsymbol{P}_{k,A}^{\star}$ and an analog combiner matrix $\boldsymbol{G}_{k,A}^{\star}$ for a certain set of subcarriers $\Omega \subset \{1, \ldots, N_{\mathrm{subc}}\}$. We consider a reduced set of subcarriers in order to reduce the computational complexity. For this sake, we modify (18) and (19) as follows

$$\left(\boldsymbol{P}_{\Omega,A}^{\star}, \boldsymbol{P}_{\Omega,D}^{\star}\right) = \underset{\boldsymbol{P}_{\Omega,A}, \boldsymbol{P}_{\Omega,D}}{\arg\min} \quad \|\boldsymbol{P}_{\Omega}^{\star} - \boldsymbol{P}_{\Omega,A}\boldsymbol{P}_{\Omega,D}\|_{\mathrm{F}} \quad \text{s.t.} \quad \|\boldsymbol{P}_{\Omega,A}\boldsymbol{P}_{\Omega,D}\|_{\mathrm{F}}^{2} \leq |\Omega| \frac{P_{\mathrm{tx}}}{N_{\mathrm{subc}}} \quad \boldsymbol{P}_{\Omega,A} \in \mathcal{P}_{\mathcal{A}}, \tag{21}$$

and

$$\left(\boldsymbol{G}_{\Omega,A}^{\star}, \boldsymbol{G}_{\Omega,D}^{\star}\right) = \underset{\boldsymbol{G}_{\Omega,A}, \boldsymbol{G}_{\Omega,D}}{\arg\min} \quad \|\boldsymbol{G}_{\Omega}^{\star} - \boldsymbol{G}_{\Omega,A}\boldsymbol{G}_{\Omega,D}\|_{\mathrm{F}} \quad \text{s.t.} \quad \boldsymbol{G}_{\Omega,A} \in \mathcal{G}_{\mathcal{A}}, \tag{22}$$

where

$$\begin{aligned}
\boldsymbol{P}_{\Omega}^{\star} &= \left[\boldsymbol{P}_{\omega_1}^{\star}, \ldots, \boldsymbol{P}_{\omega_{|\Omega|}}^{\star}\right] && \in \mathbb{C}^{N_{\mathrm{rx}} \times (|\Omega| N_{\mathrm{s}})}, \\
\boldsymbol{G}_{\Omega}^{\star} &= \left[\boldsymbol{G}_{\omega_1}^{\star}, \ldots, \boldsymbol{G}_{\omega_{|\Omega|}}^{\star}\right] && \in \mathbb{C}^{N_{\mathrm{tx}} \times (|\Omega| N_{\mathrm{s}})}, \\
\boldsymbol{P}_{\Omega,D} &= \left[\boldsymbol{P}_{\omega_1,D}, \ldots, \boldsymbol{P}_{\omega_{|\Omega|},D}\right] && \in \mathbb{C}^{N_{\mathrm{tx}}^{\mathrm{RF}} \times (|\Omega| N_{\mathrm{s}})}, \\
\boldsymbol{G}_{\Omega,D} &= \left[\boldsymbol{G}_{\omega_1,D}, \ldots, \boldsymbol{G}_{\omega_{|\Omega|},D}\right] && \in \mathbb{C}^{N_{\mathrm{rx}}^{\mathrm{RF}} \times (|\Omega| N_{\mathrm{s}})} \\
\boldsymbol{P}_{\Omega,A} &\in \mathbb{C}^{N_{\mathrm{tx}} \times N_{\mathrm{tx}}^{\mathrm{RF}}} \\
\boldsymbol{G}_{\Omega,A} &\in \mathbb{C}^{N_{\mathrm{rx}} \times N_{\mathrm{rx}}^{\mathrm{RF}}}
\end{aligned} \tag{23}$$

with $\omega_l \in \Omega$, $\forall l \in \{1, \ldots, |\Omega|\}$. Note that the per-subcarrier power constraint in (18) has been replaced by an sum power constraint in (21) in order to facilitate the calculation of the analog parts of the transceiver.

The optimization problems in (21) and (22) have the structure from equations (18) and (19) and can thus be solved with the OMP and BCD-SD algorithms described in Section IV-A. Solving (21) and (22) provides also with the corresponding digital precoding and combining matrices for the subcarriers from the set Ω. We scale them by using (20). For the subcarriers not in Ω, we propose to obtain them by the best approximation (orthogonal projection) of the optimal precoding solution by means of the analog precoding matrix found for the set Ω

$$\begin{aligned}
\boldsymbol{P}_{l,D} &= \sqrt{\frac{P_{\mathrm{tx}}}{N_{\mathrm{subc}}}} \frac{\boldsymbol{P}_{\Omega,A}^{\star,\dagger}\boldsymbol{P}_{k}^{\star}}{\left\|\boldsymbol{P}_{\Omega,A}^{\star}\left(\boldsymbol{P}_{\Omega,A}^{\star,\dagger}\boldsymbol{P}_{k}^{\star}\right)\right\|_{\mathrm{F}}} \\
\boldsymbol{G}_{l,D} &= \boldsymbol{G}_{\Omega,A}^{\star,\dagger}\boldsymbol{G}_{k}^{\star}, \\
& \quad l \in \{1, \ldots, N_{\mathrm{subc}}\} \setminus \Omega.
\end{aligned} \tag{24}$$

Both $\boldsymbol{P}_{\Omega,A}^{\star}$ and $\boldsymbol{G}_{\Omega,A}^{\star}$ are tall matrices, as $N_{\mathrm{rx}} \geq N_{\mathrm{rx}}^{\mathrm{RF}}$ and $N_{\mathrm{tx}} \geq N_{\mathrm{tx}}^{\mathrm{RF}}$. A Moore-Penrose pseudoinverse of a tall matrix $\boldsymbol{A}$ is given by $\boldsymbol{A}^{\dagger} = \left(\boldsymbol{A}^{\mathrm{H}}\boldsymbol{A}\right)^{-1}\boldsymbol{A}^{\mathrm{H}}$.

V. Simulation results

In our simulations, we use the system model from Section II and the channel model defined in (12), with parameters in Table I. We also present results from the channels measured in the measurement campaign at the Ilmenau University of Technology [29].

We define the sectorized antenna pattern for the transmitter's antenna elements as in [30, Eq. (5)]. The azimuth width of the sector is $120°$and the elevation width of the sector is $60°$. The receiver's antenna elements are omnidirectional. We notice that because of the sectorized antenna pattern much less than $\sum_{l=1}^{N_{\mathrm{cl}}} N_{\mathrm{path}}^{l}$ paths contribute to the channel. This is consistent with the principle of low-rank mmWave channels.

For sake of our simulations, we define the receive signal-to-noise ratio (SNR) as

$$\mathrm{SNR} = \frac{P_{\mathrm{tx}}}{L\sigma_{\eta}^{2}}. \tag{25}$$

The figure of merit is the achievable rate as defined in (9). We perform our simulations with 4 different transmission and reception strategies (ST), as summarized in Table II.

The results of numerical simulations are presented in Figures 2 (with BCD-SD algorithm) and 3 (with OMP algorithm), where the rates achieved with hybrid beamforming and combining (ST2-ST5) and full digital precoding and combining (ST1) are compared.

In both Fig. 2 and Fig. 3 we observe that increasing the cardinality of the set Ω leads to results closer to the baseline solution which requires an individual set of phase shifters for each subcarrier. Moreover, already with a small set of subcarriers ($|\Omega| = 1$ for the OMP decomposition and $|\Omega| = 3$ for the BCD-SD decomposition), the considered algorithm results in good system performance. The gap to the baseline rate curve is negligible. We explain the noticeable gap between the

TABLE I
TABLE OF SIMULATION PARAMETERS

Parameter	Value	Comments
N_{rx}	16	—
N_{tx}	64	—
$N_{\text{rx}}^{\text{RF}}$	4	—
$N_{\text{tx}}^{\text{RF}}$	4	—
N_{subc}	256	—
N_{s}	3	—
N_{cl}	8	Number of clusters
N_{path}^{l}	10	$\forall l \in [1,\ N_{\text{cl}}]$
$p(t)$	$\sin(\pi t)/(\pi t)$	sinc pulse
τ_l, τ_r	—	As in [25]
$\boldsymbol{\theta}_{r,l}$ (DoA)	—	Elevation: $\kappa_{r,l}^{\theta}$, azimuth: $\zeta_{r,l}^{\theta}$
$\boldsymbol{\phi}_{r,l}$ (DoD)	—	Elevation: $\kappa_{r,l}^{\phi}$, azimuth: $\zeta_{r,l}^{\phi}$
$\kappa_{r,l}^{\theta}$	$\kappa_{l}^{\text{mean},\theta} + \kappa_{r,l}^{\text{rem},\theta}$	—
$\zeta_{r,l}^{\theta}$	$\zeta_{l}^{\text{mean},\theta} + \zeta_{r,l}^{\text{rem},\theta}$	—
$\kappa_{r,l}^{\phi}$	$\kappa_{l}^{\text{mean},\phi} + \kappa_{r,l}^{\text{rem},\phi}$	—
$\zeta_{r,l}^{\phi}$	$\zeta_{l}^{\text{mean},\phi} + \zeta_{r,l}^{\text{rem},\phi}$	—
$\kappa_{l}^{\text{mean},\theta}$, $\kappa_{l}^{\text{mean},\phi}$	$\sim U[-\pi/2, \pi/2]$	—
$\zeta_{l}^{\text{mean},\theta}$, $\zeta_{l}^{\text{mean},\phi}$	$\sim U[0, 2\pi]$	—
$\kappa_{r,l}^{\text{rem},\theta}$, $\zeta_{r,l}^{\text{rem},\theta}$, $\kappa_{r,l}^{\text{rem},\phi}$, $\zeta_{r,l}^{\text{rem},\phi}$	$\sim L(0, 7.5°)$	Laplace distribution with 0 mean and standard deviation $\sigma^{\text{rem}} = 7.5°$

TABLE II
TABLE OF SIMULATED TRANSMISSION AND RECEPTION STRATEGIES

# ST	Description	Comments
ST1	Full digital setup. Linear precoding with $\boldsymbol{P}_k^{\star}$ and linear combining with $\boldsymbol{G}_k^{\star}$ for each subcarrier k	Upper bound
ST2	Hybrid transceiver structure. Linear precoding with $\boldsymbol{P}_{k,A}^{\star}\boldsymbol{P}_{k,D}^{\star}$ and linear combining with $\left(\boldsymbol{G}_{k,A}^{\star}\boldsymbol{G}_{k,D}^{\star}\right)^{\text{H}}$ for each subcarrier. Not practical - not possible with an analog beamformer common for all subcarriers.	Baseline (not practical)
ST3	Hybrid transceiver structure. Linear precoding with $\boldsymbol{P}_{\Omega,A}^{\star}\boldsymbol{P}_{k,D}^{\star}$ and linear combining with $\left(\boldsymbol{G}_{\Omega,A}^{\star}\boldsymbol{G}_{k,D}^{\star}\right)^{\text{H}}$ for each subcarrier. Practical - both the transmitter and receiver requires only one set of phase shifters in order to realize both $\boldsymbol{P}_{\Omega,A}^{\star}$ and $\boldsymbol{G}_{\Omega,A}^{\star}$ (which are constant across all the subcarriers)	$\Omega = \lceil \frac{N_{\text{subc}}}{2} \rceil$ - set containing only the central subcarrier
ST4$_n$		Ω- set containing n subcarriers, symmetrically chosen w.r.t. the central subcarrier
ST5		$\Omega = \{1, \ldots, N_{\text{subc}}\}$ (considering all subcarriers)

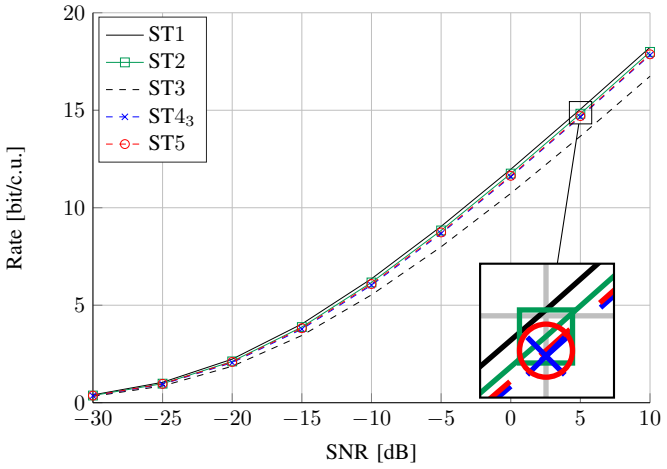

Fig. 2. Numerical evaluation of the link rates for different transmit and receive strategies defined in Table II. BCD-SD algorithm is used for decomposition of the suboptimal precoder and combiner matrices.

baseline and $|\Omega| = 1$ rate curves for BCD-SD decomposition in Fig. 2 with as follows. The OMP decomposition is taking the structure of the channel into account and is therefore more likely to find the close to optimal solution based on the channel at only one subcarrier. On the other hand, the BCD-SD algorithm is independent on the channel model.

The performance of the baseline solution with OMP is slightly worse than with the BCD-SD, since the set of available analog precoders is more restricted with the OMP algorithm compared to the BCD-SD.

Finally, Figs. 4 and 5 show results of the same simulations performed for a set of channels from the measurement campaign at the Ilmenau University of Technology [29]. Although only a limited set of measurements were available in [29], we can observe the same trend as in Fig. 3 and 2. For the practical hybrid beamforming schemes, we observe that the gap to the upper bound and the baseline case is larger compared to employing the channel model (12).

VI. CONCLUSION

We showed how common wideband analog transmit and receive beamformers can be jointly designed with per-subcarrier transmit and receive digital filters in a multi-carrier, multi-stream mmWave system. The performance of the investigated algorithms is seen to exhibit a rather small loss compared to the solutions based on a fully digital architecture, with the evaluations being performed using a statistical model as well as a set of measurement data. The loss was slightly larger with evaluation being done on measurement data. By considering the fact that the beamformers are influenced mainly by the setup geometry, the (sub)-optimized solutions can be further simplified, e.g., by considering just a subset of subcarriers for the design of the analog precoding/combining matrices. This will result in lower computational complexity of the algorithms. Future work will include the investigation of channel estimation and multi-user aspects for the assumed hybrid architecture.

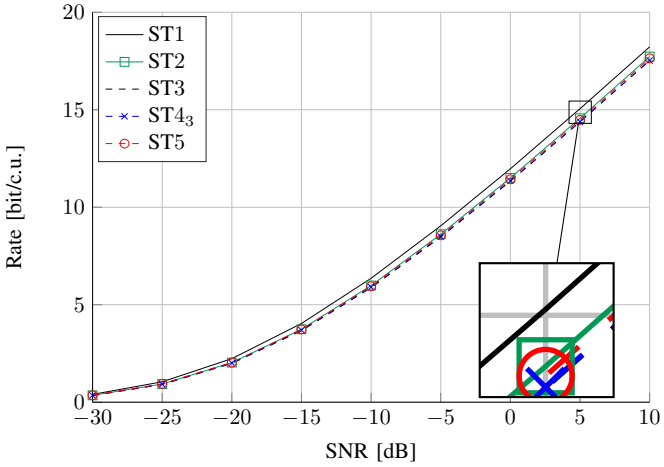

Fig. 3. Numerical evaluation of the link rates for different transmit and receive strategies defined in Table II. OMP algorithm is used for decomposition of the suboptimal precoder and combiner matrices.

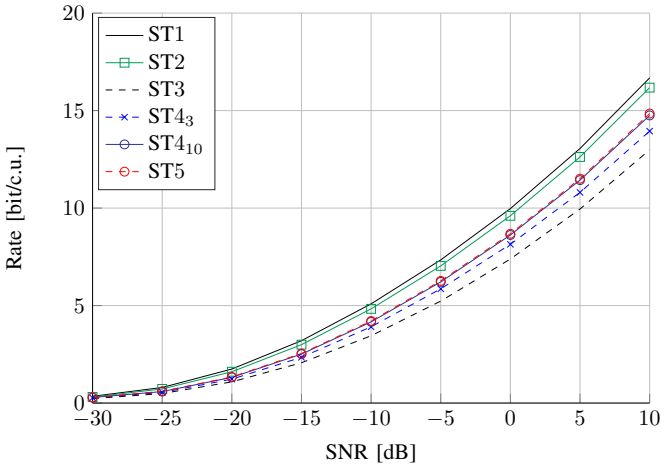

Fig. 4. Numerical evaluation of the link rates for the existing set of channel measurements for different transmit and receive strategies defined in Table II. BCD-SD algorithm is used for decomposition of the suboptimal precoder and combiner matrices.

ACKNOWLEDGEMENT

The research leading to these results received funding from the European Commission H2020 programme under grant agreement n°671650 (mmMAGIC project). The authors would also like to thank Michael Joham (Technische Universität München) for fruitful discussions.

REFERENCES

[1] Z. Pi and F. Khan, "An Introduction to Millimeter Wave Mobile Broadband Systems," *IEEE Communications Magazine*, pp. 101–107, June 2011.

[2] T. S. Rappaport, S. Sun, R. Mayzus, H. Zhao, Y. Azar, K. Wang, G. N. Wong, J. K. Schulz, M. Samimi, and F. Gutierrez, "Millimeter Wave Mobile Communications for 5G Cellular: It Will Work!" *IEEE Access*, pp. 335–349, May 2013.

[3] "NGMN 5G white paper," A Deliverable by NGMN Alliance, February 2015.

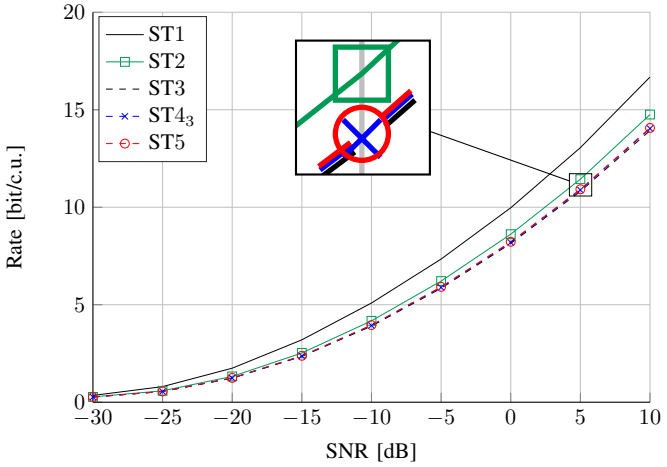

Fig. 5. Numerical evaluation of the link rates for the existing set of channel measurements for different transmit and receive strategies defined in Table II. OMP algorithm is used for decomposition of the suboptimal precoder and combiner matrices.

[4] IEEE 802.11 Working Group, "Part 11: Wireless LAN medium access control (MAC) and physical layer (PHY) specifications IEEE 802.11ad," Amendment 3: Enhancements for Very High Throughput in the 60 GHz Band, January 2012.

[5] M. Nekovee, P. von Wrycza, M. Fresia, M. Peter, J. Gora, J. Luo, and M. Tesanovic, "Millimetre-wave based mobile radio access network for fifth generation integrated communications (mmMAGIC)," in *Proc. EuCNC 2015*, Paris, France, July 2015.

[6] W. Roh, J.-Y. Seol, J. Park, B. Lee, J. Lee, Y. Ki, J. Cho, K. Cheun, and F. Aryanfar, "Millimeter-Wave Beamforming as an Enabling Technology for 5G Cellular Communications: Theoretical Feasibility and Prototype Results," *IEEE Communications Magazine*, pp. 106–113, Feb. 2014.

[7] J. Mo and R. W. Heath, "High SNR capacity of millimeter wave MIMO systems with one-bit quantization," in *in Proc. Info. Theory and Applications Wksp.*, Feb. 2014.

[8] J. Brady, N. Behdad, and A. M. Sayeed, "Beamspace MIMO for millimeter-wave communications: System architecture, modeling, analysis and measurements," *IEEE Trans. Antennas Propag.*, vol. 61, no. 7, pp. 3814–3827, July 2013.

[9] A. Alkhateeb, O. E. Ayach, G. Leus, and R. W. Heath, "Channel estimation and hybrid precoding for millimeter wave cellular systems," *IEEE J. Sel. Topics Signal Process.*, vol. 8, no. 5, pp. 831–846, Oct. 2014.

[10] A. Alkhateeb, J. Mo, N. Gonzlez-Prelcic, and R. W. Heath, "MIMO precoding and combining solutions for millimeter-wave systems," vol. 52, no. 12, Dec. 2014, pp. 12–131.

[11] S. Han, C.-L. I, Z. Xu, and C. Rowell, "Large-scale antenna systems with hybrid analog and digital beamforming for millimeter wave 5G," *IEEE Commun. Mag.*, vol. 53, no. 1, pp. 186–194, Jan. 2015.

[12] S. Noh, M. D. Zoltowski, and D. J. Love, "Downlink training codebook design and hybrid precoding in FDD massive MIMO systems," in *in IEEE Global Communications Conference (Globecom)*, Dec. 2014.

[13] L. Liang, W. Xu, and X. Dong, "Low-complexity hybrid precoding in massive multiuser MIMO systems," *IEEE Wireless Commun. Lett.*, vol. 3, no. 2, pp. 653–656, Dec. 2014.

[14] T. E. Bogale and L. B. Le, "Beamforming for multiuser massive MIMO systems: Digital versus hybrid analog-digital," *to appear, arXiv:1407.0446v2*, July 2014.

[15] R. W. Heath, N. Gonzalez-Prelcic, S. Rangan, W. Roh, and A. Sayeed, "An overview of signal processing techniques for millimeter wave MIMO systems," *to appear, arXiv:1512.03007v1*, Dec. 2015.

[16] J. Nsenga, A. Bourdoux, and F. Horlin, "Mixed analog/digital beamforming for 60GHz MIMO frequency selective channels," in *in Proc. of IEEE International Conference on Communications (ICC)*, May 2010.

[17] C. Kim, T. Kim, and J.-Y. Seol, "Multi-beam transmission diversity with hybrid beamforming for MIMO-OFDM systems," in *in Proc. of IEEE Global Communications Conference (Globecom)*, Dec. 2013, pp. 61–65.

[18] T. E. Bogale, L. B. Le, and A. Haghighat, "Hybrid analog-digital beamforming: How many RF chains and phase shifters do we need?" *submitted, arXiv:1410.2609v1*, 2014.

[19] A. Alkhateeb and R. W. Heath Jr., "Frequency selective hybrid precoding for limited feedback millimeter wave systems," *CoRR*, vol. abs/1510.00609, 2015. [Online]. Available: http://arxiv.org/abs/1510.00609

[20] C. Kim, J.-S. Son, T. Kim, and J.-Y. Seol, "On the hybrid beamforming with shared array antenna for mmWave MIMO-OFDM systems," in *in IEEE Wireless Commun. Netw. Conf. (WCNC)*, Apr. 2014, pp. 335–340.

[21] H. Ghauch, M. Bengtsson, T. Kim, and M. Skoglund, "Subspace estimation and decomposition for hybrid analog-digital millimetre-wave MIMO systems," in *in Proc. IEEE Signal Processing Advances in Wireless Communications (SPAWC)*, Stockholm, Sweden, June 2015, pp. 395–399.

[22] D. Tse and P. Viswanath, *Fundamentals of Wireless Communication*. New York, NY, USA: Cambridge University Press, 2005.

[23] Z. Wang and G. Giannakis, "Wireless multicarrier communications," *IEEE Signal Processing Magazine*, vol. 17, no. 3, pp. 29–48, May 2000.

[24] H. Bolcskei, D. Gesbert, and A. Paulraj, "On the capacity of OFDM-based spatial multiplexing systems," *IEEE Transactions on Communications*, vol. 50, no. 2, pp. 225–234, Feb. 2002.

[25] M. Samimi and T. Rappaport, "3-D statistical channel model for millimeter-wave outdoor mobile broadband communications," in *2015 IEEE International Conference on Communications (ICC)*, June 2015, pp. 2430–2436.

[26] T. Thomas, H. C. Nguyen, G. Maccartney, and T. Rappaport, "3D mmWave Channel Model Proposal," in *2014 IEEE 80th Vehicular Technology Conference (VTC Fall)*, Sep. 2014, pp. 1–6.

[27] M. Akdeniz, Y. Liu, M. Samimi, S. Sun, S. Rangan, T. Rappaport, and E. Erkip, "Millimeter Wave Channel Modeling and Cellular Capacity Evaluation," *IEEE Journal on Selected Areas in Communications*, vol. 32, no. 6, pp. 1164–1179, June 2014.

[28] M. Samimi and T. Rappaport, "Ultra-wideband statistical channel model for non line of sight millimeter-wave urban channels," in *2014 IEEE Global Communications Conference (GLOBECOM)*, Dec. 2014, pp. 3483–3489.

[29] S. Hafner, D. Dupleich, R. Muller, J. Luo, E. Schulz, C. Schneider, R. Thoma, X. Lu, and T. Wang, "Characterisation of Channel Measurements at 70GHz in Indoor Femtocells," in *2015 IEEE 81st Vehicular Technology Conference (VTC Spring)*, May 2015, pp. 1–5.

[30] O. El Ayach, S. Rajagopal, S. Abu-Surra, Z. Pi, and R. Heath, "Spatially Sparse Precoding in Millimeter Wave MIMO Systems," *IEEE Transactions on Wireless Communications*, vol. 13, no. 3, pp. 1499–1513, Mar. 2014.

[31] A. Saleh and R. Valenzuela, "A Statistical Model for Indoor Multipath Propagation," *IEEE Journal on Selected Areas in Communications*, vol. 5, no. 2, pp. 128–137, Feb. 1987.

[32] E. Biglieri, R. Calderbank, A. Constantinides, A. Goldsmith, A. Paulraj, and H. V. Poor, *MIMO Wireless Communications*. New York, NY, USA: Cambridge University Press, 2007.